

Forward-backward asymmetry of photoemission in C_{60} excited by few-cycle laser pulses

C.-Z. Gao,¹ P. M. Dinh*,¹ P.-G. Reinhard,² E. Suraud,¹ and C. Meier³

¹*Laboratoire de Physique Théorique, Université de Toulouse, CNRS, UPS, France*

²*Institut für Theoretische Physik, Universität Erlangen, Staudtstraße 7, D-91058 Erlangen, Germany*

³*Laboratoire Collisions-Agrégats-Réactivité, Université de Toulouse, CNRS, UPS, France*

(Dated: March 10, 2022)

We theoretically analyze angle-resolved photo-electron spectra (ARPES) generated by the interaction of C_{60} with intense, short laser pulses. In particular, we focus on the impact of the carrier-envelope phase (CEP) onto the angular distribution. The electronic dynamics is described by time-dependent density functional theory, and the ionic background of C_{60} is approximated by a particularly designed jellium model. Our results show a clear dependence of the angular distributions onto the CEP for very short pulses covering only very few laser cycles, which disappears for longer pulses. For the specific laser parameters used in a recent experiments, a very good agreement is obtained. Furthermore, the asymmetry is found to depend on the energy of the emitted photo-electrons. The strong influence of the angular asymmetry of electron emission onto the CEP and pulse duration suggests to use this sensitivity as a means to analyze the structure of few-cycle laser pulses.

PACS numbers:

I. INTRODUCTION

With the advance in laser technology, it has become possible to generate femtosecond laser pulses which cover only few optical cycles [1, 2], and this has rapidly found a broad range of applications in many disciplines, such as the generation of attosecond pulses and precision control of chemical process. In this context, one of the most intriguing aspects is that these extremely short pulses may give access to time-resolved electronic dynamics in atoms and molecules. This paves the way to a multiplicity of interesting phenomena, such as high-order harmonic generation (HHG), above-threshold ionization (ATI), and laser-induced molecular fragmentation, as has been seen already in several earlier experimental and theoretical studies [2–9], for reviews see Refs. [10–13]. It has also been shown that structural information of the target can be retrieved using short light pulses [14, 15].

The carrier-envelope phase (CEP) is the phase of the fast oscillations of the laser field relative to its envelope. For few-cycle lasers, this CEP becomes a decisive laser parameter because the CEP offsets modify the pattern of the pulse dramatically, which, in turn, can have a strong impact on laser-induced electron dynamics. For example, photoelectron emission induced by few-cycle laser fields can be controlled by the CEP, leading to a pronounced forward-backward (also called “right-left”) asymmetry in the photoelectron spectra (PES). This has been experimentally reported in [16] where it was found that the outcome depends on the photoelectrons’ kinetic energy. The energy dependence has been explained within a semi-classical model by different electron emission processes in

the low- and high-energy regimes [17]. In the low-energy regime, electrons are directly emitted with a kinetic energy of up to the $2U_p$, where $U_p = I_{\text{las}}/4\omega_{\text{las}}^2$ (in atomic units) is the ponderomotive energy of the laser field.

In the high-energy regime, electron recollision with the target system dominates, forming a plateau-like structure in the PES delimited by a well-defined cutoff. The rescattered electrons can be accelerated to energies of roughly up to the $10U_p$ [18] provided that the tail of the laser field is still sufficiently high which is, however, rather critical for few-cycle laser fields. Interestingly, a couple of theoretical calculations have shown that the parts of PES related to electron recollisions are more sensitive to CEP than those parts related to electrons emitted directly [5, 9, 19–21]. Experimentally, the dependence of high-energy PES on the CEP has been explored for atoms, e.g., xenon [16, 22], argon [23], krypton [22], as well as for small-sized dimer molecules, e.g., N_2 and O_2 [24]. Recently, it has been studied in solids, such as tungsten [25] and gold nanotips [26] which were found to be efficient and controllable nanoemitters of extreme ultraviolet (XUV) electrons, thus allowing to investigate ultrafast electron dynamics in solids at an attosecond time scale, for a recent review see Ref. [27].

Compared to atoms and dimers, the C_{60} fullerene is a typical example for a large system on the way from molecules to solids. Thus the study of C_{60} might help toward understanding dynamical properties of nanosystems. The advantage of C_{60} is its stability and accessibility which renders it a useful laboratory for the study, e.g., of thermal electron emission, charge migration, fragmentation channels, HHG, and ATI, see Refs. [28–31]. From a geometrical point of view, C_{60} is similar to the outermost part of capped-carbon nanotips which are promising XUV electron nanoemitters. In a previous work [32], we have theoretically investigated the PES of C_{60} in strong

*corresponding author : dinh@irsamc.ups-tlse.fr

fields using a near-infrared laser pulse ($\lambda_{\text{las}}=912$ nm). In that study, CEP effects were neglected since we considered comparatively long pulses comprising about 8 optical cycles. Recently, experiments on C_{60} using intense few-cycle infrared laser pulses (720 nm and 4 fs) [33] were reported, in which a dramatic dependence of the PES on CEP was observed and qualitatively reproduced by Monte Carlo (MC) and Quantum Dynamical (QD) simulations.

The aim of this article is to study the dependence of the PES on the CEP for C_{60} illuminated by intense, infrared, few-cycle laser pulses in a fully quantum-mechanical framework. Our modeling is based on Time-Dependent Density-Functional Theory [34] with the time-dependent local-density approximation using the jellium approximation for the ionic background [32]. We will focus on the dependence of the CEP effect on pulse length and on the forward-backward asymmetry of photoemission due to electron rescattering.

The paper is outlined as follows, Section II briefly describes the theoretical approach and the numerical analysis. Results are presented and analyzed in Section III. Finally, conclusions are summarized in Section IV.

II. FORMAL FRAMEWORK

We describe the electronic dynamics of C_{60} by time-dependent density functional theory (TDDFT) at the level of the time-dependent local density approximation (TDLDA) [35] using the exchange-functional from [36]. For an appropriate modeling of electron emission, we augment TDLDA by a self-energy correction (SIC) [37]. As a full SIC treatment is computationally cumbersome [38], we use it in a simplified, but reliable and efficient version as an average density SIC (ADSIC) [39]. The ADSIC suffices to put the single-particle energies into right relation to continuum threshold such that the ionization potential (IP) is correctly reproduced in a great variety of systems [40] from simple atoms to large organic molecules. In this context, a correct description of IP is crucial for photoemission excited by external fields, in particular by strong fields as it is assumed to be dominated by electrons in the highest occupied molecular orbitals (HOMO) [41].

The ionic background (here carbon ions) is modeled within the jellium approximation by a sphere of positive charge with a void at the center [42–44]. The jellium potential reads (in atomic units) :

$$v_{\text{jel}}(\mathbf{r}) = - \int d^3\mathbf{r}' \frac{\rho_{\text{jel}}(|\mathbf{r}'|)}{|\mathbf{r} - \mathbf{r}'|} + v_{\text{ps}}(|\mathbf{r}|), \quad (1a)$$

$$\rho_{\text{jel}}(r) = \rho_0 g(r), \quad (1b)$$

$$v_{\text{ps}}(r) = v_0 g(r), \quad (1c)$$

$$g(r) = \frac{1}{1 + e^{(r-R_-)/\sigma}} \frac{1}{1 + e^{(R_+-r)/\sigma}}, \quad (1d)$$

$$R_{\pm} = R \pm \frac{\Delta R}{2}. \quad (1e)$$

Here g denotes the Woods-Saxon profile, providing a soft transition from bulk shell to the vacuum. The jellium potential (v_{jel}) is augmented by an additional potential v_{ps} which is tuned to obtain reasonable values of the single-particle energies [45]. The shell radius R is taken from experimental data as $R = 6.7 a_0$ [46]. The other parameters are the same as those in Ref. [32]. With the present scheme, we reproduce rather well the electronic properties of C_{60} : an IP at $E_{\text{IP}} = 7.62$ eV, a HOMO-LUMO gap of 1.77 eV, and a reasonable description of the photo-absorption spectrum [45]. This is in nice agreement with experimental values [47, 48].

It should be noted that the bulk density ρ_0 is determined such that $\int d^3\mathbf{r} \rho_{\text{jel}}(\mathbf{r}) = N_{\text{el}} = 238$. Note that this number of electrons is different from 240 for a real C_{60} . This is because no jellium model so far manages to place the electronic shell at $N_{\text{el}} = 240$ as it should be. Most have the closure at $N_{\text{el}} = 250$ [42–44]. The present model with soft surfaces comes to $N_{\text{el}} = 238$ which is much closer to the reality. Nevertheless, we have to keep in mind that a jellium model is a rough approximation to a detailed ionic structure. But it is a powerful approximation as it allows to appropriately describe many features of electronic structure and dynamics in solids [49, 50] and cluster physics, see Refs. [51, 52]. Recently, the present model has been validated as one of efficient and reliable tools to describe electron recollisions in strong fields in C_{60} , see Ref. [32]. The jellium model stands naturally for a frozen ionic background. It is justified for the present study where the laser pulses considered are so short that the nuclear dynamics can be neglected.

Within the dipole approximation, and assuming a linearly polarized laser pulse with the polarization vector along the z -axis \mathbf{e}_z , the interaction with the laser field (in atomic units) is given by

$$v_{\text{las}}(r, t) = E(t) \mathbf{r} \cdot \mathbf{e}_z \quad (2)$$

with the electric field chosen to be

$$E(t) = E_0 \cos^2\left(\frac{\pi t}{T_{\text{las}}}\right) \cos(\omega_{\text{las}} t + \phi_{\text{CEP}}) \quad (3)$$

for $-T_{\text{las}}/2 \leq t \leq T_{\text{las}}/2$. Here, E_0 denotes the peak electric field, ω_{las} the carrier frequency, and T_{las} the total pulse duration. The CEP is comprised in the parameter ϕ_{CEP} which defines the phase between oscillations at frequency ω_{las} and the maximum of the \cos^2 envelope. In what follows, we use laser parameters close to those in recent experiments [33]: laser frequency $\omega_{\text{las}} = 1.72$ eV (a wavelength of 720 nm), intensity $I = 6 \times 10^{13}$ W/cm², corresponding to field amplitude $E_0 = 1.1$ eV/ a_0 , and total duration $T_{\text{las}}=4$ fs, 6 fs, and 8 fs, corresponding to 1.7, 2.5, and 3.3 optical cycles (1 optical cycle = 2.4 fs). Note that these laser parameters are associated with a ponderomotive energy $U_p = 2.9$ eV. Figure 1 illustrates the temporal part of the laser field for the three T_{las} under consideration, each one for the CEP at 0° (black curves) and 90° (red curves). For $\phi_{\text{CEP}} = 0^\circ$, the center of the

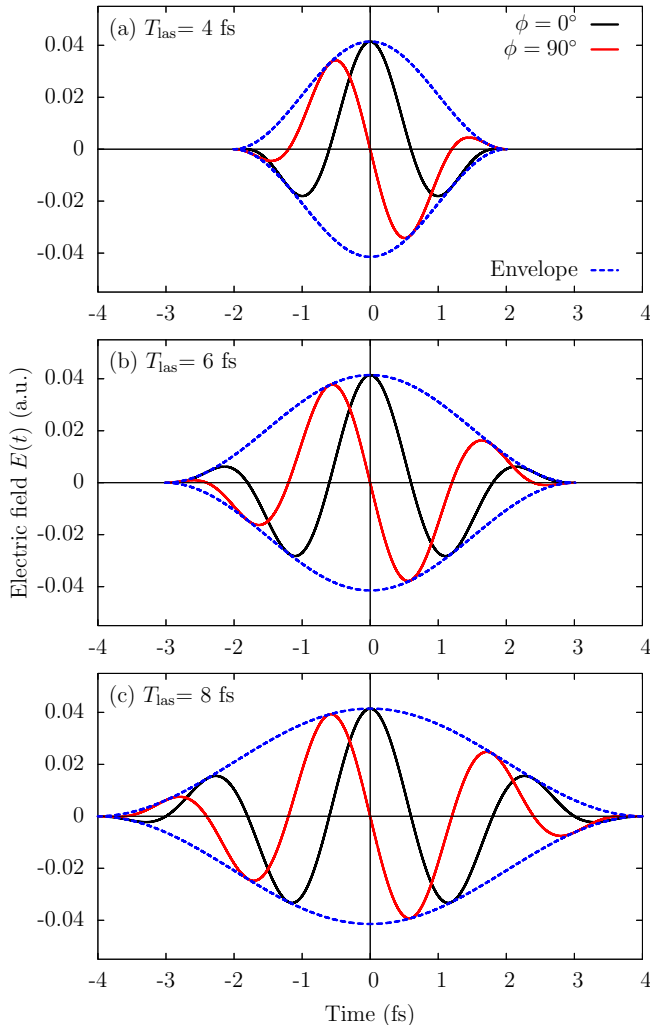


Figure 1: (Color online) The temporal part of the laser field (3) for $T_{\text{las}}=4$ fs (a), 6 fs (b), 8 fs (c). Each panel is plotted at $\phi_{\text{CEP}} = 0^\circ$ (black lines) and 90° (red lines). The envelope is shown in dashed blue lines. Horizontal ($E=0$) and vertical ($t=0$) solid lines are depicted to facilitate the CEP comparison. Other laser parameters are given in the text.

envelope coincides with a maximum of the oscillations, while for $\phi_{\text{CEP}} = 90^\circ$, it is shifted to match with the nodal points of the electric field. Clearly, we see a substantial change of the electric field due to the different CEP in each case.

A. Numerical details

The TDLDA equations are solved numerically on a cylindrical grid in coordinate space [53]. The static iterations towards the electronic ground state are done with the damped gradient method [54] and time evolution employs the time-splitting technique [55]. For details of the numerical methods, see [56–58]. We use a numerical box which extends $500 a_0$ in z direction (along the laser polar-

ization) and $250 a_0$ orthogonal to it (radial r coordinate), with a grid spacing of $0.5 a_0$ in both directions. Time propagation is followed up to after 44 fs with a small time step of 10^{-3} fs. Box size and time span are sufficiently large to track completely the rescattering of electrons in the laser field (ponderomotive motion). To account for ionization, absorbing boundary conditions are implemented using a mask function [59]. The absorbing margin extends over $35 a_0$ (70 grid points) at each side.

The central observable of electron emission in our analysis are angle-resolved photoelectron spectra (ARPES), i.e., the yield of emitted electrons $[\mathcal{Y}(E_{\text{kin}}, \theta)]$ as function of kinetic energy E_{kin} and emission angle θ . We calculate ARPES by recording at each time step the single-electron wave functions $\{\psi_j(t, \mathbf{r}_{\mathcal{M}}), j = 1, \dots, N_{\text{el}}\}$ at selected measuring points $\mathbf{r}_{\mathcal{M}}$ near the absorbing layer and finally transforming this information from time- to frequency-domain, see [60–63]. Finally, the PES is written as

$$\mathcal{Y}(E_{\text{kin}}, \theta) \propto \sum_{j=1}^{N_{\text{el}}} |\widetilde{\psi}_j(E_{\text{kin}}, \mathbf{r}_{\mathcal{M}})|^2 \quad (4)$$

where $\widetilde{\psi}_j$ are the transformed wave functions in energy domain. In case of strong fields, as we encounter here, the $\widetilde{\psi}_j$ are to be augmented by a phase factor accounting for the ponderomotive motion, for technical details see [62]. The angle θ is defined with respect to \mathbf{e}_z , i.e. $\theta = 0^\circ$ means electronic emission in the direction of \mathbf{e}_z . A detailed ARPES analysis requires a fine resolution. To that end, we use an increment of 0.04 eV in energy and 1° for the angular bins.

III. RESULTS AND DISCUSSIONS

A. CEP-averaged PES

We first look at CEP-averaged photoelectron spectra, simply denoted by PES, of C_{60} in a forward emission cone as measured in the experiments of [33]. The computed PES are thus averaged over CEP in a range of 0° - 360° with $\Delta\phi_{\text{CEP}} = 15^\circ$ and collected in a forward cone with opening angle of 15° . Figure 2 shows the calculated results for the three pulse lengths together with the experimental results (black solid circles) [33]. The patterns of the CEP-averaged PES are found to depend sensitively on the pulse length T_{las} . At low energies ($6 \leq E_{\text{kin}} \leq 25$ eV), the photoelectron yield decreases with increasing T_{las} . It is interesting to note that the PES for $T_{\text{las}}=4$ fs reaches a maximum around 10 eV. This coincides approximately with $3.2U_p$ which is the maximal energy upon the first return of rescattered electrons. A similar pattern has been obtained in C_{60} by quantum dynamical (QD) calculations [33] under the same laser conditions. For the longest pulse considered, $T_{\text{las}}=8$ fs, we find pronounced peaks which are the ATI peaks separated by the photon energy. For shortest pulse lengths,

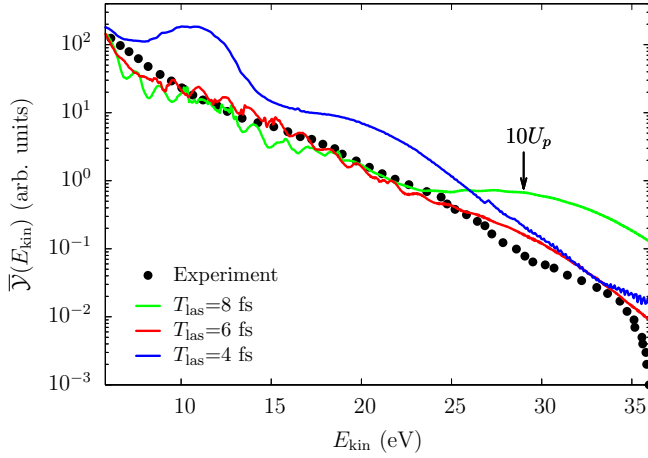


Figure 2: (Color online) CEP-averaged photoelectron spectra (PES) of C_{60} excited by intense, linearly polarized, few-cycle laser pulses. Experimental data [33] are shown as black circles and calculated results as full curves for different pulse lengths as indicated. The PES are collected in a cone with opening angle of 15° at a fixed CEP and then averaged over a CEP range of 0° - 360° at a step of $\Delta\phi_{\text{CEP}}=15^\circ$. The high-energy cutoff position at $10U_p$ is indicated by a black arrow.

these structures vanish because the pulse does not have sufficient energy resolution any more. In the high-energy regime ($25 \leq E_{\text{kin}} \leq 36$ eV), we see a reverse dependence on T_{las} , where the longest pulse ($T_{\text{las}}=8$ fs) leads to the highest yield because there is more time to accelerate emitted electrons in the still ongoing laser field. The most satisfactory agreement between TDLDA results and experimental data is found for $T_{\text{las}}=6$ fs, which can nearly reproduce the measured PES data in the full energy range. This strong dependence of PES on pulse length may provide an opportunity to characterize the experimental pulse duration by comparing the pattern of PES to calculated results.

B. Angle-resolved PES (ARPES)

In a next step, we analyze the full ARPES at fixed CEP values for the pulse length $T_{\text{las}}=6$ fs where computed CEP-averaged PES agree best with experiments, as seen in the previous section. Figure 3 shows ARPES for two typical CEP values, $\phi_{\text{CEP}} = 0^\circ$ in panel (a) and 90° in (b). The most prominent feature in both cases is the remarkable $\theta = 0^\circ \leftrightarrow 180^\circ$ asymmetry of the PES, particularly for electrons in the high-energy regime ($E_{\text{kin}} \geq 25$ eV). At $\phi_{\text{CEP}} = 0^\circ$ in Fig. 3(a), high-energy photoelectrons are emitted favorably in the direction towards $\theta = 180^\circ$, which is characterized by a rather broad ramp extending to 35 eV. In contrast, low-energy electrons ($6 \leq E_{\text{kin}} \leq 15$ eV) are emitted preferentially towards $\theta = 0^\circ$. The observed ARPES pattern is consistent with angular-integrated asymmetry maps in experiments [33] for the CEP analyzed here. The preferences of

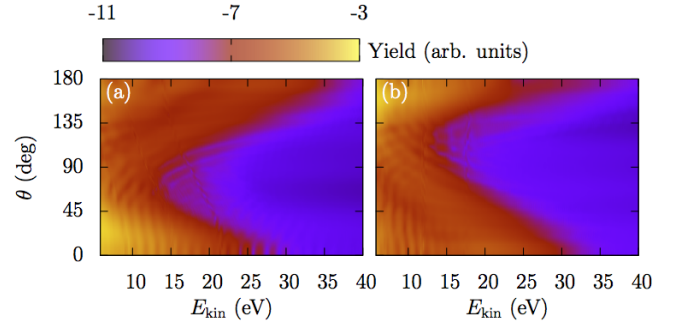


Figure 3: (Color online) ARPES of C_{60} excited by a pulse with duration $T_{\text{las}}=6$ fs, frequency $\omega_{\text{las}} = 1.72$ eV, and intensity $I_{\text{las}} = 6 \times 10^{13}$ W/cm 2 for $\phi_{\text{CEP}} = 0^\circ$ (a) and 90° (b).

electron emission change for $\phi_{\text{CEP}} = 90^\circ$ in Fig. 3(b), in which the low-energy electrons have more weight towards $\theta = 180^\circ$ while the high-energy electrons prefer the other way towards $\theta = 0^\circ$. A similar asymmetry of the PES is also observed for $T_{\text{las}} = 4$ fs and 8 fs (not shown). The example demonstrates that strong few-cycle laser pulses can effectively control the ARPES.

This behavior has been observed also in experiments for xenon atoms [16] and has been theoretically analyzed in [5, 19] based on the strong-field approximations and on the integration of three-dimensional time-dependent Schrödinger equation. A semiclassical explanation is that the generation of high-energy electrons originate from the electron recolliding with the target, thus depending on the two time instants at which electrons were released and scattered off, respectively. It is difficult for few-cycle laser pulses to fulfill this condition simultaneously in $\theta = 0^\circ$ and 180° directions. However, it is possible to realize it in one of the two directions by tuning the CEP offset of the laser field, as shown in Fig. 3. This has been first suggested in [2] as a phase-meter to determine the absolute phase of an ultrashort laser pulse. We shall show in the next step that such a phase-meter strongly depends on pulse duration and that it becomes invalid with increasing pulse length.

C. Asymmetry versus CEP

The dominant feature of the ARPES in Fig. 3 is the strong influence of CEP on the energy resolved forward-backward asymmetry. This was also found in the previous work where the asymmetry often produces regular oscillations for the CEP as function of kinetic energy [12]. To investigate such oscillations for the present example, we define the asymmetry η as

$$\eta(\phi_{\text{CEP}}) = \frac{\mathcal{Y}(E_{1-2}, \theta^+) - \mathcal{Y}(E_{1-2}, \theta^-)}{\mathcal{Y}(E_{1-2}, \theta^+) + \mathcal{Y}(E_{1-2}, \theta^-)} \quad (5)$$

where E_{1-2} denotes in brief the integration in the energy interval $[E_1 : E_2]$ and θ^+ and θ^- stand for cones of emis-

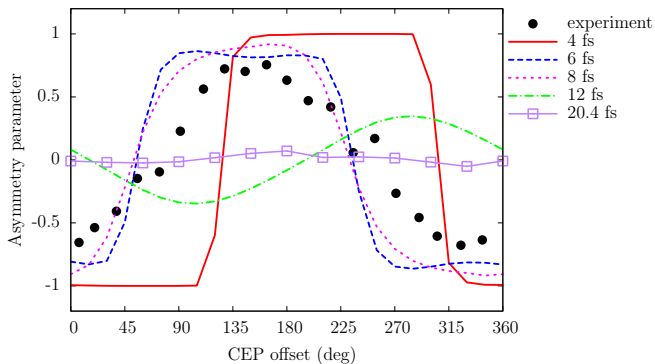


Figure 4: (Color online) Comparison of the asymmetry parameter η , see Eq. (5), from experiments [33] (black solid circles) with theoretical results (red solid curves for $T_{\text{las}} = 4$ fs, blue dashes for 6 fs, magenta dots for 8 fs, green dash-dotted curves for 12 fs, and purple open squares for 20.4 fs). All cases have been integrated in the same range of kinetic energies $[E_1 : E_2] = [23 \text{ eV} : 30.6 \text{ eV}]$ as done in experiments.

sion angles. In most experiments, photoelectron yields are collected in a cone angle of 15° . This means that θ^+ corresponds to $|\theta^+| \leq 15^\circ$ and θ^- to $|180 - \theta^-| \leq 15^\circ$. We use the same convention for our theoretical analysis.

Figure 4 compares the asymmetry parameter η between experiments (black solid circles) [33] and calculated results for various pulse lengths T_{las} . We find a good agreement between experimental data and present results for $T_{\text{las}} = 6$ fs (blue dashes) as well as 8 fs (magenta dots) regarding the width and position of the maxima of $\eta(\phi_{\text{CEP}})$. Yet, slight differences remain for the shape of $\eta(\phi_{\text{CEP}})$. The experimental curve shows softer transitions than the two theoretical curves. The \cos^2 envelope of the theoretical pulse, see Eq. (3), is surely more confined than the experimental pulse which is often assumed to have Gaussian envelope, but may easily be plagued by prepulses [64].

The pattern of $\eta(\phi_{\text{CEP}})$ differ substantially from the experiment for other T_{las} (smaller than 6-8 fs and larger ones) concerning position of maxima/minima, amplitude of oscillations, and softness on T_{las} . Clear trends are seen for the amplitude which decreases with increasing T_{las} and the softness which increases with T_{las} , both together eventually wiping out the signal for long pulses. The trends are plausible. Very short pulse shrink basically to one oscillation and so become extremely sensitive to the CEP while more and more comparably high oscillations in longer pulses render the CEP less crucial. This strong sensitivity of the signal $\eta(\phi_{\text{CEP}})$ to pulses parameters raises the question how sensitive the result is to details of the pulse profile. To check that, we have also run calculations with a Gaussian envelope for the laser pulse instead of the \cos^2 envelope used above, see Eq. (3). The results are practically the same if the same FWHM is used. Therefore, we conclude that pulse length is the decisive parameter and measuring $\eta(\phi_{\text{CEP}})$ can give access to this parameter. However, η emerges from combined

action of laser pulses and responding system. This aspect, i.e., the influence of the system, will be addressed in future work.

Although it is plausible that the impact of CEP fades away for longer pulses, CEP-dependent asymmetry of the PES can be recovered also for longer pulses by a collinear, two-color pump-probe scheme, namely, a combination of a fundamental laser (ω) and its n -th order harmonic ($n\omega$) typically represented by a ω - 2ω laser setup. The presence of a second harmonic is used to twist the field strength of the fundamental mode by varying the delay phase, resulting in the asymmetry in the field amplitude influencing ionization as well as the rescattering. The ω - $n\omega$ scheme has previously been proposed in [65], and has later been used to explore the PES asymmetry in sodium clusters (Na_4 and Na_4^+) excited by intense 7-cycle laser fields [66]. A more recent experimental application of ω - 2ω combined laser pulses on rare gas atoms and CO_2 molecule is found in Ref. [67]. On this basis, the comparison of controlling efficiency of CEP-dependent asymmetry between one-color few-cycle fields and two-color multiple-cycle fields is an intriguing topic, yet this is beyond the scope of present study, thus we postpone it to the next exploration.

Since the asymmetry parameter (5) depends on the kinetic energy of the photoelectrons, it is also interesting to study its dependence on the energy. Figure 5 shows η as a function of the kinetic energy and the ϕ_{CEP} , using $T_{\text{las}} = 6$ fs. As most striking result, we find the the anisotropy parameter strongly depends both on the CEP and the kinetic energy of the emitted photoelectrons. For high energy electrons, i.e., between ~ 23 and ~ 30 eV, we find the strong CEP dependence already visible in Fig. 4. For low energy electrons, those less than ~ 15 eV, we find an opposite behavior. This reflects the complex electron

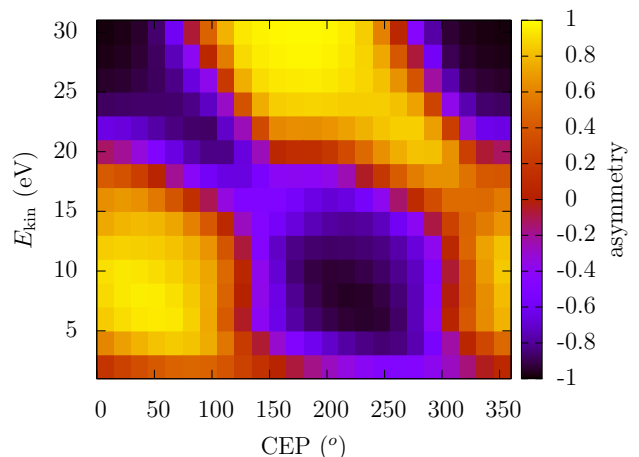


Figure 5: (Color online) Dependence of the asymmetry parameter on the CEP and on the kinetic energy of the emitted electrons (for $T_{\text{las}} = 6$ fs). A strong CEP dependence is found, with opposite behavior for low (< 15 eV and high energy electrons (between 23 eV and 31 eV).

dynamics taking place during the interaction with the ultrashort laser pulse, which changes drastically for different CEP's.

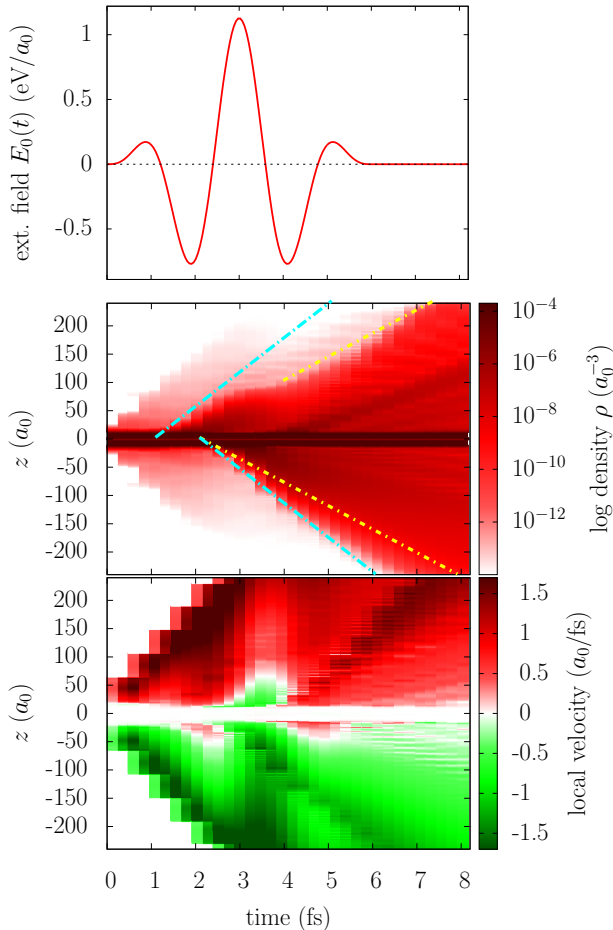


Figure 6: Time evolution of external field (upper panel), local density along z -axis (middle panel), and local velocity along z -axis (lower panel) for C_{60} excited by a laser pulse with a duration of $T_{\text{las}}=6$ fs, frequency $\omega_{\text{las}} = 1.72$ eV, intensity $I_{\text{las}} = 6 \times 10^{13} \text{W}/\text{cm}^2$, and CEP $\phi_{\text{CEP}} = 0^\circ$. The cyan lines in the density plot (middle panel) indicate a velocity $\pm v = 58 a_0/\text{fs}$ corresponding to a kinetic energy of 13.6 eV and the yellow lines of $\pm v = 41 a_0/\text{fs}$ corresponding to 27.2 eV.

To explain these features in more detail, we have analyzed the electron dynamics in the case of $\phi_{\text{CEP}} = 0^\circ$. These results are depicted in Fig. 6. It shows the time evolution of the density (middle panel) and the velocity distribution (bottom panel), together with the electric field of the laser pulse (top panel). In analyzing the results, one has to concentrate on the low-density tail corresponding to the finally emitted flow. The velocities need to be looked together with the density because velocity alone does not indicate the importance of a contribution (which is weighted, of course, with the density). As soon as the electric field sets on, both the density and the velocity show oscillations synchronous with the external field. A bunch of high positive velocities (cyan line with positive

slope) develops followed by a density shift to positive z short after the first negative peak in E_0 at 2 fs. This turns into opposite direction following the strong positive peak in E_0 after 3 fs and a last swap back with the counter peak after 4 fs. A particularly interesting process takes place with the largest peak at 3 fs. The negative peak before has triggered a strong flow to positive z . This is abruptly stopped and counter-weighted by the subsequent large positive field (exerting a force in the negative direction). The positive flow recovers only with the second negative E_0 peak and leaves the system with a kinetic energy of about 13.6 eV (yellow line with positive slope). The large positive peak, on the other hand, releases a bunch of fast electrons towards negative direction which escapes eventually with the higher kinetic energy of 27.2 eV (cyan line with negative slope). The detailed time-resolved picture so nicely elucidates the peaks on 0° and 180° direction in the previous figure.

IV. CONCLUSIONS

We have investigated the impact of the carrier-envelope phase (CEP) of very short laser pulses on the angle-resolved photo-electron spectra (ARPES) of the C_{60} cluster. To this end, we used as a tool time-dependent density-functional theory at the level of the time-dependent local-density approximation. This was augmented by self-interaction correction to achieve a correct ionization potential which is crucial for an appropriate description of photoemission dynamics. The ionic background is assumed to be frozen during the femtosecond dynamics. For C_{60} , it is approximated by a jellium model which is particularly tuned to its special geometry. Absorbing boundary conditions are used to describe electron emission and ARPES are computed with sampling the time evolution of the single-electron wave functions at selected measuring points close to the absorbing margins.

Our results depend sensitively on the laser pulse length. This holds already for the global signal of CEP-averaged photo-electron spectra where we find a good agreement with experimental results when using the appropriate pulse length (and huge deviations from data for other pulse lengths). Particular attention was paid to the angular asymmetry of ARPES. A short glance at the full ARPES distribution and a detailed evaluation of asymmetry as a function of energy show that the asymmetry behaves different in low- and high-energy regime. This is explained in detail by analyzing the time-dependent density and velocity distributions of the accelerated electrons.

Following experimental data, we have focused then on the dependence of asymmetry on CEP in the regime of high-energy emission. For very short pulses, we find a strongly varying function oscillating with steep slopes between the forward/backward extremes of asymmetry. These patterns change significantly with the pulse pa-

rameters. The amplitude of oscillations shrinks with increasing pulse length while the pattern become softer. In particular, the signal practically disappears for longer pulses covering 8 laser cycles or more. We find again a good agreement with experimental data for the appropriate pulse length, the same which also allowed to reproduce the CEP-averaged photo-electron spectra.

We have studied the sensitivity of the results to the detailed profile of the laser pulse (Gaussian versus \cos^2). The differences are so small that pulse profiles cannot be identified clearly from the asymmetry signal.

This study emphasizes the amount of detailed information that can be gained from a systematic scan of the ARPES as a function of the CEP. For example, the high sensitivity of asymmetry versus CEP to the laser pulse may be used for an independent measurement of pulse parameters. This may constitute an interesting aspect for ultrashort pulse characterization. However, in order to develop the shown methodology in this direction, one

needs to carefully disentangle pulse properties from system properties, as resonances. Research along these lines are currently being undertaken.

Acknowledgments:

We thank Institut Universitaire de France, European ITN network CORINF and French ANR contract LASCAR (ANR-13-BS04-0007) for support during the realization of this work. One of authors (C.-Z.G.) is grateful for the financial support from China Scholarship Council (CSC) (No. [2013]3009). It was also granted access to the HPC resources of CalMiP (Calcul en Midi-Pyrénées) under the allocation P1238, and of RRZE (Regionales Rechenzentrum Erlangen).

-
- [1] M. Nisoli, S. De Silvestri, O. Svelto, R. Szipöcs, K. Ferencz, C. Spielmann, S. Sartania, and F. Krausz, *Opt. Lett.* **22**, 522 (1997).
 - [2] G. Paulus, F. Grasbon, H. Walther, P. Villorosi, M. Nisoli, S. Stagira, E. Priori, and S. De Silvestri, *Nature* **414**, 182 (2001).
 - [3] G. Tempea, M. Geissler, and T. Brabec, *JOSA B* **16**, 669 (1999).
 - [4] A. Baltuška, T. Udem, M. Uiberacker, M. Hentschel, E. Goulielmakis, C. Gohle, R. Holzwarth, V. Yakovlev, A. Scrinzi, T. Hänsch, et al., *Nature* **421**, 611 (2003).
 - [5] S. Chelkowski and A. D. Bandrauk, *Phys. Rev. A* **71**, 053815 (2005).
 - [6] M. Kling, C. Siedschlag, A. J. Verhoef, J. Khan, M. Schultze, T. Uphues, Y. Ni, M. Uiberacker, M. Drescher, F. Krausz, et al., *Science* **312**, 246 (2006).
 - [7] Y. Liu, X. Liu, Y. Deng, C. Wu, H. Jiang, and Q. Gong, *Phys. Rev. Lett.* **106**, 073004 (2011).
 - [8] X. Xie, K. Doblhoff-Dier, S. Roither, M. S. Schöffler, D. Kartashov, H. Xu, T. Rathje, G. G. Paulus, A. Baltuška, S. Gräfe, et al., *Phys. Rev. Lett.* **109**, 243001 (2012).
 - [9] N. Suárez, A. Chacón, M. F. Ciappina, J. Biegert, and M. Lewenstein, *Phys. Rev. A* **92**, 063421 (2015).
 - [10] T. Brabec and F. Krausz, *Rev. Mod. Phys.* **72**, 545 (2000).
 - [11] W. Becker, F. Grasbon, R. Kopold, D. Milosevic, G. Paulus, and H. Walther, *Adv. Atom Mol. Opt. Phys.* **48**, 35 (2002).
 - [12] D. Milošević, G. Paulus, D. Bauer, and W. Becker, *J. Phys. B: At. Mol. Opt. Phys.* **39**, R203 (2006).
 - [13] S. Haessler, J. Caillat, and P. Salieres, *J. Phys. B: At. Mol. Opt. Phys.* **44**, 203001 (2011).
 - [14] T. Morishita, A.-T. Le, Z. Chen, and C. D. Lin, *Phys. Rev. Lett.* **100**, 013903 (2008).
 - [15] H. Kang, W. Quan, Y. Wang, Z. Lin, M. Wu, H. Liu, X. Liu, B. B. Wang, H. J. Liu, Y. Q. Gu, et al., *Phys. Rev. Lett.* **104**, 203001 (2010).
 - [16] G. G. Paulus, F. Lindner, H. Walther, A. Baltuška, E. Goulielmakis, M. Lezius, and F. Krausz, *Phys. Rev. Lett.* **91**, 253004 (2003).
 - [17] P. B. Corkum, *Phys. Rev. Lett.* **71**, 1994 (1993).
 - [18] G. G. Paulus, W. Becker, W. Nicklich, and H. Walther, *J. Phys. B: At. Mol. Opt. Phys.* **27**, L703 (1994).
 - [19] D. Milošević, G. Paulus, and W. Becker, *Opt. Express* **11**, 1418 (2003).
 - [20] X. M. Tong, K. Hino, and N. Toshima, *Phys. Rev. A* **74**, 031405 (2006).
 - [21] Q. Liao, P. Lu, P. Lan, W. Cao, and Y. Li, *Phys. Rev. A* **77**, 013408 (2008).
 - [22] M. Kling, J. Rauschenberger, A. Verhoef, E. Hasović, T. Uphues, D. Milošević, H. Muller, and M. Vrakking, *New J. Phys.* **10**, 025024 (2008).
 - [23] F. Lindner, M. G. Schätzel, H. Walther, A. Baltuška, E. Goulielmakis, F. Krausz, D. B. Milošević, D. Bauer, W. Becker, and G. G. Paulus, *Phys. Rev. Lett.* **95**, 040401 (2005).
 - [24] A. Gazibegović-Busuladžić, E. Hasović, M. Busuladžić, D. B. Milošević, F. Kelkensberg, W. K. Siu, M. J. J. Vrakking, F. Lépine, G. Sansone, M. Nisoli, et al., *Phys. Rev. A* **84**, 043426 (2011).
 - [25] M. Krüger, M. Schenk, and P. Hommelhoff, *Nature* **475**, 78 (2011).
 - [26] D. J. Park, B. Piglosiewicz, S. Schmidt, H. Kollmann, M. Mascheck, and C. Lienau, *Phys. Rev. Lett.* **109**, 244803 (2012).
 - [27] M. Krüger, M. Schenk, M. Förster, and P. Hommelhoff, *J. Phys. B: At. Mol. Opt. Phys.* **45**, 074006 (2012).
 - [28] I. Hertel, T. Laarmann, and C. Schulz, *Adv. Atom Mol. Opt. Phys.* **50**, 219 (2005).
 - [29] E. E. Campbell, K. Hansen, M. Hedén, M. Kjellberg, and A. V. Bulgakov, *Photochem. Photobiol. Sci.* **5**, 1183 (2006).
 - [30] R. Ganeev, *Laser Phys.* **21**, 25 (2011).
 - [31] F. Lépine, *J. Phys. B: At. Mol. Opt. Phys.* **48**, 122002 (2015).
 - [32] C.-Z. Gao, P. M. Dinh, P. Klüpfel, C. Meier, P.-G. Reinhard, and E. Suraud, *Phys. Rev. A* **93**, 022506 (2016).

- [33] H. Li, B. Mignolet, G. Wachter, S. Skruszewicz, S. Zharebtsov, F. Süßmann, A. Kessel, S. Trushin, N. G. Kling, M. Kübel, et al., *Phys. Rev. Lett.* **114**, 123004 (2015).
- [34] E. Runge and E. K. Gross, *Phys. Rev. Lett.* **52**, 997 (1984).
- [35] R. M. Dreizler and E. K. U. Gross, *Density Functional Theory: An Approach to the Quantum Many-Body Problem* (Springer-Verlag, Berlin, 1990).
- [36] J. P. Perdew and Y. Wang, *Phys. Rev. B* **45**, 13244 (1992).
- [37] J. P. Perdew and A. Zunger, *Phys. Rev. B* **23**, 5048 (1981).
- [38] J. Messud, P. M. Dinh, P.-G. Reinhard, and E. Suraud, *Ann. Phys. (N.Y.)* **324**, 955 (2008).
- [39] C. Legrand, E. Suraud, and P.-G. Reinhard, *J. Phys. B: At. Mol. Opt. Phys.* **35**, 1115 (2002).
- [40] P. Klüpfel, P. M. Dinh, P.-G. Reinhard, and E. Suraud, *Phys. Rev. A* **88**, 052501 (2013).
- [41] H.-G. Müller and M. Fedorov, *Super-intense laser-atom physics IV*, vol. 13 (Springer Science & Business Media, 1996).
- [42] M. Puska and R. M. Nieminen, *Phys. Rev. A* **47**, 1181 (1993).
- [43] D. Bauer, F. Ceccherini, A. Macchi, and F. Cornolti, *Phys. Rev. A* **64** (2001).
- [44] E. Cormier, P.-A. Hervieux, R. Wiehle, B. Witzel, and H. Helm, *Eur. Phys. J. D* **26**, 83 (2003).
- [45] P.-G. Reinhard, P. Wopperer, P. M. Dinh, and E. Suraud, in *ICQNM 2013, The Seventh International Conference on Quantum, Nano and Micro Technologies* (2013), pp. 13–17.
- [46] K. Hedberg, L. Hedberg, D. S. Bethune, C. A. Brown, H. C. Dorn, R. D. Johnson, and M. de Vries, *Science* **254**, 410 (1991).
- [47] D. L. Lichtenberger, M. E. Jatcko, K. W. Nebesny, C. D. Ray, D. R. Huffman, and L. D. Lamb, *Mater. Res. Soc. Symp. Proc.* **206**, 673 (1990).
- [48] K. Sattler, *Handbook of Nanophysics: Clusters and Fullerenes*, Handbook of Nanophysics (CRC Press, 2010).
- [49] N. W. Ashcroft and N. D. Mermin, *Solid State Physics* (Saunders College, Philadelphia, 1976).
- [50] C. Lemell, X.-M. Tong, F. Krausz, and J. Burgdörfer, *Phys. Rev. Lett.* **90**, 076403 (2003).
- [51] U. Kreibig and M. Vollmer, *Optical properties of metal clusters*, vol. 25 (Springer Science & Business Media, 2013).
- [52] M. Brack, *Rev. Mod. Phys.* **65**, 677 (1993).
- [53] B. Montag and P.-G. Reinhard, *Z. Phys. D: At., Mol. Clusters* **33**, 265 (1995).
- [54] P.-G. Reinhard and R. Cusson, *Nucl. Phys. A* **378**, 418 (1982).
- [55] M. Feit, J. Fleck, and A. Steiger, *J. Comput. Phys.* **47**, 412 (1982).
- [56] F. Calvayrac, P.-G. Reinhard, E. Suraud, and C. A. Ullrich, *Phys. Rep.* **337**, 493 (2000).
- [57] P.-G. Reinhard and E. Suraud, *Introduction to Cluster Dynamics* (Wiley, New York, 2003).
- [58] P. Wopperer, P. M. Dinh, P.-G. Reinhard, and E. Suraud, *Phys. Rep.* **562**, 1 (2015).
- [59] P.-G. Reinhard, P. D. Stevenson, D. Almhed, J. A. Maruhn, and M. R. Strayer, *Phys. Rev. E* **73**, 036709 (2006).
- [60] A. Pohl, P.-G. Reinhard, and E. Suraud, *J. Phys. B* **34**, 4969 (2001).
- [61] U. De Giovannini, D. Varsano, M. A. L. Marques, H. Appel, E. K. U. Gross, and A. Rubio, *Phys. Rev. A* **85**, 062515 (2012).
- [62] P. M. Dinh, P. Romaniello, P.-G. Reinhard, and E. Suraud, *Phys. Rev. A* **87**, 032514 (2013).
- [63] M. Dauth and S. Kümmel, *Phys. Rev. A* **93**, 022502 (2016).
- [64] A. Giuliani, P. Tomassini, M. Galimberti, D. G. L. A. Gizzi, P. Koester, L. Labate, T. Ceccotti, P. D’Azevedo, T. Auguste, P. Monot, et al., *Phys. Plasmas* **13**, 093103 (2006).
- [65] G. Paulus, W. Becker, and H. Walther, *Phys. Rev. A* **52**, 4043 (1995).
- [66] H. Nguyen, A. Bandrauk, and C. A. Ullrich, *Phys. Rev. A* **69**, 063415 (2004).
- [67] S. Skruszewicz, J. Tiggesbäumker, K.-H. Meiwes-Broer, M. Arbeiter, T. Fennel, and D. Bauer, *Phys. Rev. Lett.* **115**, 043001 (2015).